Studying the Electron Charge to Mass Ratio With a Pair of Helmholtz Coils

Sara Parvaresh Rizi (1010913451), Aarya Shah (1010871157)

January 20, 2026

1 Abstract

In this experiment, the charge-to-mass ratio of an electron is investigated by analyzing the trajectory and radius of an electron as it passes through a pair of Helmholtz coils. The calculated external magnetic field, B_e is $(-1.1 \pm 0.2) \times 10^{-4}$ µT, almost twice as high as the Earth's magnetic field in Toronto, with opposite polarity. The charge-to-mass ratio of an electron was found to be between $(3.5 \pm 0.2) \times 10^{11} C/kg$ and $(9.7 \pm 0.9) \times 10^{10} C/kg$, with percent differences around 100% and 45% respectively. The electrons through the coils shifted under the influence of a ferromagnetic object, which was more apparent in circles with a smaller radius.

2 Introduction

In the presence of a magnetic field($\vec{B}$, magnitude B), a particle with charge e and mass m deflects upon experiencing a force ($\vec{F}$), given by (Zhan, Horsley, and Harlick 2025).

$$\vec{F} = e\vec{v} \times \vec{B} \tag{1}$$

Under a constant $\vec{B}$, the particle moves in a closed circular orbit of radius r. The curvature of the electron orbit (r) under a potential difference ΔV is found by

$$\frac{1}{r} = \sqrt{\frac{e}{2m}} \frac{B}{\sqrt{\Delta V}} \tag{2}$$

In this experiment, $\vec{B}$ is generated by the current (I) through a pair of Helmholtz coils (see Figure 1). The radius of each coil R and the coil separation are equal, thus stabilizing the magnetic field B near the centre of the pair of coils. For $\mu_0 = 4\pi \times 10^{-7} TmA^{-1}$ and distance z, B is thus found to be

$$B = \frac{\mu_0 I R^2}{2(R^2 + z^2)^{3/2}} \tag{3}$$

Over a volume with a geometrical coil of the configuration, the magnetic field from the coils are

$$B_c = (\frac{4}{5})^{3/2} \frac{\mu_0 n I}{R} \tag{4}$$

where n is the number of turns in each coil. The total axial magnetic field is uniform, being a sum of the field from the coils and the external field of Earth, as

$$\vec{B} = \vec{B_c} + \vec{B_e} \tag{5}$$

Using Equation 5 to expand for B_c and Equation 2, the resulting equation is

$$\frac{1}{r} = \sqrt{\frac{e}{m}} k_c \frac{I + \frac{1}{\sqrt{2}} I_0}{\sqrt{\Delta V}} \tag{6}$$

or, alternatively,

$$\frac{\sqrt{\Delta V}}{r} = \sqrt{\frac{e}{m}} k_c (I + \frac{1}{\sqrt{2}} I_0) \tag{7}$$

where $k_c = \frac{1}{\sqrt{2}} (\frac{4}{5})^{3/2} \frac{\mu_0 n}{R}$ is the characteristic of coil dimensions and $I_0 = \frac{B_e}{k_c}$ is a constant proportional to the external magnetic field. In this experiment, we utilize these relations to investigate the charge-to-mass ratio of an electron through a pair of Helmholtz coils, as well as determine the effects of external magnetic fields on our setup.

3 Materials and Methods

The methods in this lab report adhere to the guidelines outlined in the 'Charge-to-mass ratio' manual (Zhan, Horsley, and Harlick 2025). Figure 1 is a labeled apparatus lab setup.

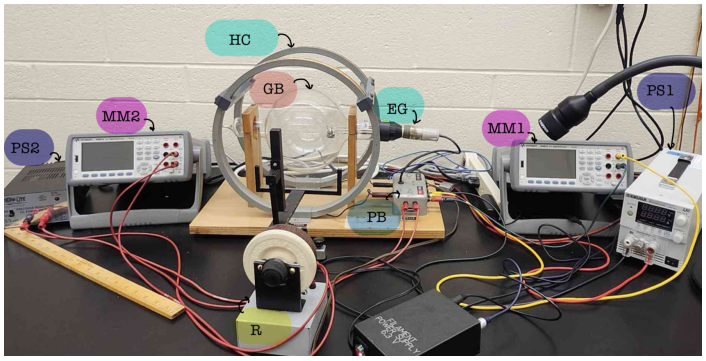

Figure 1: A photo of the experimental apparatus, where EG is the electron gun, GB the glass bulb, HC the Helmholtz coils, MM1 the anode voltage meter, MM2 the coil current meter, PB the power box, PS1 the anode and filament power supply, PS2 the coils power supply, and R the rheostat

The experimental apparatus consists of a glass bulb (GB) containing an electron gun (EG), positioned between two Helmholtz coils (HC). All system power is routed through a central power box (PB). Electrons are emitted from a hot filament and accelerated through an anode by a 0–300V DC power supply (PS1), while a 6.3V AC source from the same unit powers the filament. The magnetic field is generated by a current from an 8V DC power supply (PS2) connected in series with a rheostat (R) and an ammeter (MM2).

To begin, the filament power supply was activated for 30 seconds to allow for thermal stabilization. Following this, the anode voltage and Helmholtz coil power were turned on. In a darkened environment, the electron beam becomes visible as electrons excite the low-pressure hydrogen gas. The GB was

rotated to reorient the magnetic field, ensuring the electrons followed a closed, circular path instead of a helical trajectory.

Measurements were taken with a self-illuminated scale and plastic reflector. To eliminate parallax, the image of the electron beam (seen through the glass) was aligned at the halfway point of the HC, with its reflection on the plastic reflector. Thus, the eye position was adjusted until the beam and its reflection coincided, and the viewer's line of sight was perfectly perpendicular to the electron orbit. This ensures the scale measurement accurately represents the diameter of the path without perspective error. Furthermore, a camera was aligned directly in front of the scale to capture the readings. The camera ensured the viewer's position was constant, thus reducing parallax from eye movements. Two primary datasets were collected: one maintaining a constant accelerating potential (ΔV) while varying current (I), and another maintaining a constant current while varying potential.

4 Data and Analysis

Table 1 shows the current measurements under a constant voltage of $300V$. It shows the radius of the path of the electron decreasing with increasing current. Increasing the coil current strengthens the magnetic field, reducing the radius of curvature for a fixed electron speed.

Current ($\pm 0.001\mathbf{A}$)	**Radius** ($\pm 0.05cm$)
1.174	5.75
1.483	4.28
1.788	3.53
2.257	2.65

Table 1: Radius measurements for a changing current for the electron trajectory at a constant voltage of $300V$. The ammeter readings were noisy up to $0.001A$, prompting the error.

Similarly, the voltage measurements taken during a constant amperage of $2.187A$ are shown in Table 2.

Voltage ($\pm 0.001V$)	**Distance** ($\pm 0.05cm$)
367.241	3.28
249.940	2.60
199.976	2.00
149.740	1.90

Table 2: Radius measurements for a changing voltage for the electron trajectory at a constant current of $2.187A$. The voltmeter readings were noisy up to $\pm 0.001V$, creating the error.

By rearranging Equation 7, the ratio $\frac{e}{m}$ was found by correlating the Equation in Figure 2 with

$$B_c = \alpha \frac{1}{r} - B_e \tag{8}$$

where $\alpha = \sqrt{\frac{2m}{e}\Delta V}$. Using Equation 8, the data from Table 1, and given $n = 130$ turns from the apparatus, B_c was determined and used to find the background magnetic field. These values are shown in Figure 2.

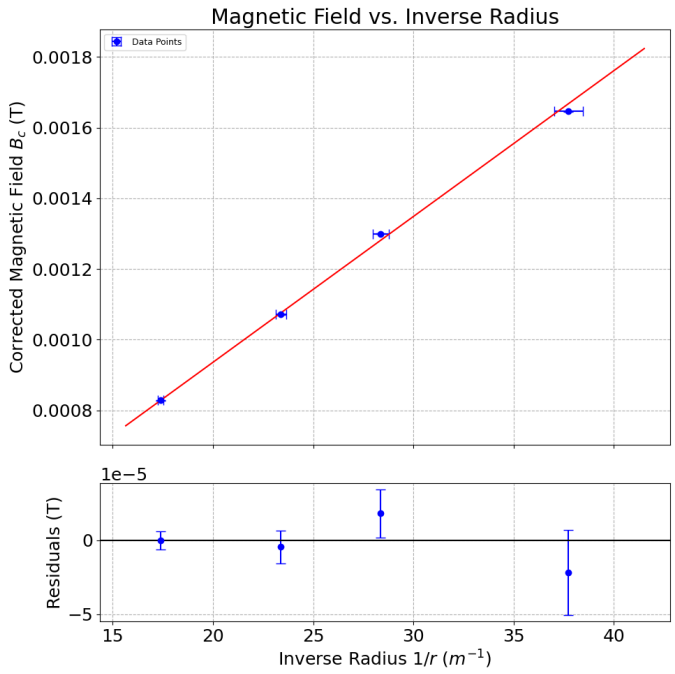

Figure 2: Linear fit (top) and residual plot (bottom) of B_c according to Equation 8, using the correction in Equation 9. The equation of the line is $B_c = (4.1 \pm 0.1) \times 10^{-5}(\frac{1}{r}) + (1.1 \pm 0.2) \times 10^{-4}$ Tesla. The mean residual was -2.1×10^{-6} T with a standard deviation of 1.4×10^{-5} T. Some vertical and horizontal error bars in the figure are too small to see.

For radii where $0.2R < \rho < 0.5R$, the B field value should be adjusted by

$$\frac{B(\rho)}{B(0)} = 1 - \frac{\rho^4}{R^4(0.6583 + 0.29\frac{\rho^2}{R^2})^2} \tag{9}$$

for $\rho = r$ in this scenario (Zhan, Horsley, and Harlick 2025). Since $R = 16$ cm, and the radii recorded all fall within this range, we apply this correction. The error propagation for B_c is outlined in Appendix 6.1.

The reduced chi-squared for Figure 2 is 0.990, suggesting the model is consistent with uncertainties in the data, and the residuals (deviations) are exactly what is expected based on the estimated measurement errors, and on average, each data point lies just within its designated error bar of the fitted line.

The y-intercept of the linear plot in Figure 2 gives the value for $-B_e$, according to Equation 8 which is $(1.1 \pm 0.2) \times 10^{-4}$ Tesla. The Earth's magnetic field is around $25 - 60$ µT, and around 55 µT in Toronto (Government of Canada n.d.). This means that $B_e = (1.1 \pm 0.2) \times 10^{-4}$ µT achieves a value that has, in magnitude, a percent difference of 101.450%, but is opposite in direction the Earth's (Kale 2026).

Given the value of $\alpha = (4.1 \pm 0.1) \times 10^{-5} Tm, \Delta V = 300.000V \pm 0.001V$, $\frac{e}{m}$ is

$$\frac{e}{m} = (3.5 \pm 0.2) \times 10^{11} C/kg$$

This value has a percent difference of 100.370% from the charge-to-mass ratio of $1.758820 \times 10^{11} C/kg$ (Byjus 2011).

Another way of calculating this ratio is by rearranging Equation 7 in the form $y = mx + b$ to take the form

$$\sqrt{\Delta V} = \left[\sqrt{\frac{e}{m}} k_c \left(I + \frac{I_0}{\sqrt{2}}\right)\right] r \tag{10}$$

By plotting $\sqrt{\Delta V}$ on the y-axis and the radius r on the x-axis, from the data in Table 2, $\frac{e}{m}$ can be extracted from the slope, given $k_c = \frac{1}{\sqrt{2}}(\frac{4}{5})^{3/2}\frac{\mu_0 n}{R} = (5.17 \pm 0.02) \times 10^{-4} T m A^{-1}$, and $I_0 = \frac{B_e}{k_c}$ from previous calculations. The calculations for error are done in Appendix 6.2.

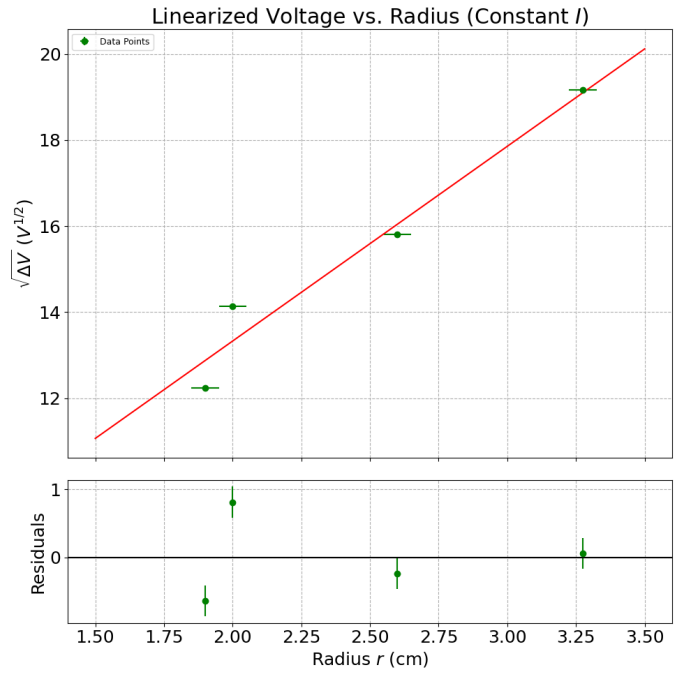

Figure 3: Linear fit (top) and residual plot (bottom) of Equation 10. The equation of the line is $\sqrt{\Delta V} = (4.5 \pm 0.2) \times 10^2 (r) + (4.3 \pm 0.5) V^{0.5} m^{-1}$. The mean residual was $-1.5 \times 10^{-9} V^{0.5}$ with a standard deviation of $0.5 V^{0.5} m^{-1}$. Some vertical error bars in the linear fit are too small to see.

From applying the slope in Equation 10, the calculated

$$\frac{e}{m} = (9.7 \pm 0.9) \times 10^{10} C/kg$$

This yields a percent error of 44.660%, which is a 55.710% decrease from the previous method. The chi-squared value is 11.000, suggesting that the model is a poor representation of the data, or that the uncertainties in the data were significantly underestimated.

5 Discussion and Conclusion

The two calculated values for the electron charge-to-mass ratio $\frac{e}{m} = \eta$ are $\eta_1 = (3.5 \pm 0.2) \times 10^{11}$ C/kg and $\eta_2 = (9.7 \pm 0.9) \times 10^{10}$ C/kg, deviate from the literature value of 1.758820×10^{11} C/kg by $\approx 100\%$ and $\approx 45\%$ respectively. While Table 1 showed a reduced chi-squared near unity, the high $\chi^2 \approx 11$ for Table 2 suggests that uncertainties were underestimated or dominated by systematic drifts. The dominant uncertainties were systematic, arising from voltmeter charging, coil heating, and geometric misalignment, rather than random measurement noise.

A primary candidate for systemic sources of error is likely the voltmeter "charging effect" mentioned in the manual, where charge accumulation causes fluctuations in the recorded ΔV. Additionally, thermal heating in the rheostat during Table 2 trials could cause a current drift, creating a non-constant magnetic field B_c not reflected in the ammeter readings. Geometrical misalignments also play a significant role; if the glass bulb is not perfectly centered, the off-axis distance ρ varies non-uniformly throughout the path, breaking the symmetry assumed in Equation 7 and even the correction factor in Equation 9.

The calculated external field $B_e = (1.1 \pm 0.2) \times 10^{-4}$ T is roughly twice the magnitude of Earth's magnetic field in Toronto (50 μT), indicating significant local magnetic contributions beyond the geomagnetic field. The positive intercept (and negative B_e) from Figure 2 implies the local background field was oriented anti-parallel to the coils' axial field. This environmental sensitivity was confirmed by the significant beam deflection observed when a ferromagnetic object was introduced.

At the highest possible current and low voltages ($\Delta V <$ 145 V), creating strong magnetic fields, the beam dimmed significantly as electrons lacked the kinetic energy to be excited. These lower velocities made the beam more susceptible to forming helical paths rather than circular ones, indicating that small velocity components parallel to the magnetic field (due to bulb misalignment) became dominant. This shows that not all parts of the trajectory were impacted, as the electron trajectory was visible when it shone towards the back of the GB, but was unable to form the ring structure. As well, note that a helical circle has velocity that is both parallel and perpendicular to the electron's motion, and because radius is proportional to the perpendicular velocity, a lower velocity would yield a smaller electron charge to mass ratio.

While we assume a uniform field B_c at the center, the field actually decreases as the electron moves away from the central axis (ρ increases), creating varied electron trajectories. Meanwhile, under a constant voltage, higher currents caused a decrease in ring radius (see Table 1. This could be because as current increases and accelerating voltage decreases, the resistance faced by the conducting wire, and thus the electrons decreases, prompting a smaller trajectory as they have greater velocity (*Power and brightness of bulbs* 2024). It was noted that as the radius decreases, helices begin to form (no longer a perfect circle), and the bulb needs to be readjusted.

Restoring a circular path required manual bulb rotation based on visual intuition rather than precise measurement, which introduced systematic bias and slight deviations from a perfect perpendicular orbit. Furthermore, the convex geometry of the glass bulb likely caused the path to appear optically larger than its physical dimensions. Furthermore, the convex geometry of the glass bulb likely caused the orbit to appear optically larger than its true dimensions. Because

$\frac{e}{m} \propto 1/r^2$, even a slight overestimation of r leads to a significantly lower calculated ratio, as can be seen in the second method.

Despite the systematic uncertainties, the experiment successfully demonstrated the prediction of circular electron motion and highlighted the sensitivity of charge-to-mass measurements to experimental alignment and environmental magnetic fields. Future iterations of this experiment could be improved by using a digital camera with a telecentric lens to eliminate optical distortion and by increasing the designated uncertainty in r to ± 0.1 cm to better reflect the finite width of the electron beam.

References

Byjus (2011). *Charge to mass ratio of electron - J J Thomson's Experiment — Chemistry*. Byjus.com. URL: https://byjus.com/chemistry/charge-to-mass-ratio/.

Government of Canada, Natural Resources Canada (n.d.). *Secular variation*. geomag.nrcan.gc.ca. URL: https://geomag.nrcan.gc.ca/mag_fld/sec-en.php.

Kale, Andy (2026). *The Earth's Field*. Carisma.ca. URL: https://carisma.ca/backgrounder/the-earth-s-field (visited on 01/16/2026).

PHY224H1F/324H1S Notes on Error Analysis (n.d.). PHY294, p. 7. URL: https://q.utoronto.ca/courses/425903/files/41245781?module_item_id=7398038.

Power and brightness of bulbs (2024). IOPSpark. URL: https://spark.iop.org/power-and-brightness-bulbs.

Zhan, H., E. Horsley, and A. Harlick (2025). *Charge-to-mass ratio for the electron*. University of Toronto Department of Physics. URL: https://www.physics.utoronto.ca/~phy224_324/LabManuals/ChargeToMassRatio.pdf.

6 Appendix

6.1 Error Propagation For B_c

Note that we use B_c with the corrected magnetic field such that $B_c = B_{ideal}(I) \cdot B_p(r)$, with $B_{ideal} = (\frac{4}{5})^{3/2}\frac{\mu_0 nI}{R}$, $B_p = 1 - \frac{\rho^4}{R^4(0.6583+0.29\frac{\rho^2}{R^2})^2}$. Therefore, the error propagation for $B_c = B_{ideal} * B_\rho$ is

$$\Delta B_c = \sqrt{(\frac{\partial B_c}{\partial I}\Delta I)^2 + (\frac{\partial B_c}{\partial r}\Delta r)^2} \tag{11}$$

where $\frac{\partial B_c}{\partial I} = \frac{B_c}{I}$ and $\frac{\partial B_c}{\partial r} = \frac{\partial B_\rho}{\partial r} = -\frac{4kR^2r^3}{(kR^2+mr^2)^3}$ for k=0.6538, m=0.29. Therefore, Equation 11 can be rewritten as

$$\Delta B_c = B_c\sqrt{\left(\frac{\Delta I}{I}\right)^2 + \left(\frac{1}{B_p}\frac{\partial B_p}{\partial r}\Delta r\right)^2}$$

or even

$$\Delta B_c = B_c\sqrt{(\frac{\Delta I}{I})^2 + (\frac{-4kR^2r^3}{B_\rho(kR^2+mr^2)^3}\Delta r)^2} \tag{12}$$

for $\Delta I = \pm 0.001A, \Delta r = \pm 0.05cm$

6.2 Error Propagation for $\frac{e}{m}$

Method 1: Using the calculation of B_c from the slope, $\frac{e}{m}$ has error propagated through Equation 7, giving

$$\frac{\Delta(e/m)}{e/m} = \sqrt{\left(\frac{\Delta(\Delta V)}{\Delta V}\right)^2 + \left(2\frac{\Delta\alpha}{\alpha}\right)^2} \tag{13}$$

Where $\Delta(\Delta V) = 0.001V$, $\Delta\alpha$ is the standard error in calculating slope, outlined in *PHY224H1F/324H1S Notes on Error Analysis* n.d.

Method 2: Using the voltage and radius dependence, let $S = \sqrt{\frac{e}{m}}k_c\left(I + \frac{I_0}{\sqrt{2}}\right)$, the slope. To find the charge-to-mass ratio, let $\eta = e/m$ and $\sqrt{\eta} = \frac{S}{k_c(I+\frac{I_0}{\sqrt{2}})}$ turns to $\eta = \frac{S^2}{k_c^2(I+\frac{I_0}{\sqrt{2}})^2}$. This lets us quickly see that our expression is a product of powers, therefore, the error is given by

$$\frac{\Delta(e/m)}{e/m} = \sqrt{\left(2\frac{\Delta S}{S}\right)^2 + \left(2\frac{\Delta k_c}{k_c}\right)^2 + \left(2\frac{\Delta(I+\frac{I_0}{\sqrt{2}})}{I+\frac{I_0}{\sqrt{2}}}\right)^2}$$

Because k_c is proportional to R, $\frac{\Delta k_c}{k_c} = \frac{\Delta R}{R}$. As well, if we let $C = I + \frac{I_0}{\sqrt{2}}$, we can apply addition rule and propagate from here. We can express our final uncertainty as

$$\frac{\Delta(e/m)}{e/m} = \sqrt{\left(2\frac{\Delta S}{S}\right)^2 + \left(2\frac{\Delta R}{R}\right)^2 + \left(\frac{2\sqrt{(\Delta I)^2 + (\Delta I_0/\sqrt{2})^2}}{I+\frac{I_0}{\sqrt{2}}}\right)^2} \tag{14}$$

where ΔS is uncertainty in the slope, ΔR is the measurement uncertainty of the Helmholtz coil radius (± 0.05 cm), ΔI is the ammeter precision (± 0.001 A), ΔI_0 is the uncertainty in the equivalent external field current, determined from the B_e y-intercept.